

Atomic Gold Ions Clustered with Noble Gases: Helium, Neon, Argon, Krypton, and XenonPaul Martini,¹ Lorenz Kranabetter,¹ Marcelo Goulart,¹ Bilal Rasul,^{1,2} Michael Gatchell,^{1,3} Paul Scheier,^{1*} Olof Echt^{1,4*}¹ Institut für Ionenphysik und Angewandte Physik, Universität Innsbruck, Technikerstr. 25, A-6020 Innsbruck, Austria² Department of Physics, University of Sargodha, 40100 Sargodha, Pakistan³ Department of Physics, Stockholm University, 106 91 Stockholm, Sweden⁴ Department of Physics, University of New Hampshire, Durham NH 03824, USA

* Corresponding authors:

Paul Scheier <paul.scheier@uibk.ac.at>

Olof Echt <olof.echt@unh.edu>

ORCID IDs:

Olof Echt 0000-0002-0970-1191

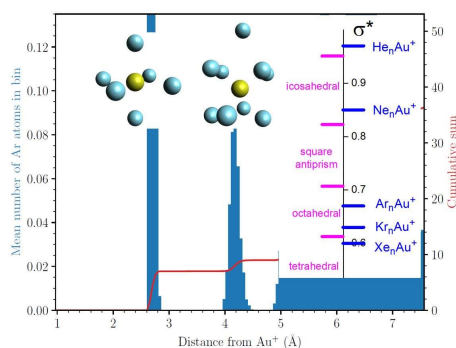
Michael Gatchell 0000-0003-1028-7976

Marcelo Goulart 0000-0002-6006-9339

Paul Scheier 0000-0002-7480-6205

Abstract

High-resolution mass spectra of helium droplets doped with gold and ionized by electrons reveal He_nAu^+ cluster ions. Additional doping with heavy noble gases results in Ne_nAu^+ , Ar_nAu^+ , Kr_nAu^+ , and Xe_nAu^+ cluster ions. The high stability predicted for covalently bonded Ar_2Au^+ , Kr_2Au^+ , and Xe_2Au^+ is reflected in their relatively high abundance. Surprisingly, the abundance of Ne_2Au^+ which is predicted to have zero covalent bonding character and no enhanced stability features a local maximum, too. The predicted size and structure of complete solvation shells surrounding ions with essentially non-directional bonding depends primarily on the ratio σ^* of the ion-ligand *versus* the ligand-ligand distance. For Au^+ solvated in helium and neon the ratio σ^* is slightly below 1, favoring icosahedral packing in agreement with a maximum observed in the corresponding abundance distributions at $n = 12$. He_nAu^+ appears to adopt two additional solvation shells of I_h symmetry, containing 20 and 12 atoms, respectively. For Ar_nAu^+ , with $\sigma^* \approx 0.67$, one would expect a solvation shell of octahedral symmetry, in agreement with an enhanced ion abundance at $n = 6$. Another anomaly in the ion abundance at Ar_9Au^+ matches a local maximum in its computed dissociation energy.



Graphic for Table of Content

1. Introduction

In 1995 Pyykkö predicted that Au^+ forms chemical bonds with the heavy noble gases (Ng) argon, krypton, and xenon.¹ For XeAu^+ , the most strongly bound diatomic, Pyykkö calculated a bond energy $D_e = 0.91$ eV, over half of it coming from relativistic effects. For $[\text{XeAuXe}]^+$ he computed an atomization energy of 2.25 eV and a bond length approaching the sum of the covalent radii of Xe and Au, respectively. Read and Buckingham questioned the need to invoke covalent bonding, arguing that inclusion of dispersion and higher order polarization effects will account for strong bonding.²

The nature of the bond in neutral and cationic $\text{NgAu}^{0,+}$ is still being debated;³⁻⁵ it has even been argued that it is a distinct kind of bond.⁶ The strength of the bond in XeAu^+ , however, is beyond doubt. Schröder et al. published coupled cluster calculations of XeAu^+ with single and double excitations and a perturbative treatment of the triples (CCSD(T)) with full counterpoise corrections that resulted in a dissociation energy $D_e = 1.31$ eV.⁷

The bond energy and bond length of neutral and charged $\text{NgAu}^{\pm,0}$ (as well as $\text{NgAg}^{\pm,0}$ and $\text{NgCu}^{\pm,0}$) have been the subject of numerous other high-level theoretical studies;⁸⁻¹⁷ also see the recent review by Pan et al.¹⁸ One interesting, widely shared conclusion is that physical interaction is sufficient to explain bonding in the weakly bound HeAu^+ and NeAu^+ ($D_e = 0.048$ eV and 0.070 eV, respectively⁹) but that increasingly larger amounts of covalent bonding and charge transfer are required to explain the bond in ArAu^+ , KrAu^+ , and XeAu^+ ($D_e = 0.464$, 0.763 and 1.25 eV, respectively⁹).

However, experimental data are scarce. Kapur and Müller identified NeAu^+ in mass spectra of electric field-evaporated ions.¹⁹ Schröder et al. detected XeAu^+ and Xe_2Au^+ in mass spectra by reacting Au^+ with C_6F_6 in the presence of xenon.⁷ Neutral NeAu , ArAu , KrAu , and XeAu have been studied by resonance enhanced multiphoton absorption (see ref. 13 and references therein) and photodissociation.²⁰ Photoelectron spectra of NgAu^- (Ng = Ne, Ar, Kr, Xe) in the gas phase have been reported by Gao et al.²¹ Also worth mentioning are experiments in which vibrational spectra of small, neutral Au_n or mixed Au_nAg_m clusters complexed with a few krypton²² or argon²³ atoms were recorded; the data indicated very strong interaction between gold clusters and noble gas atoms.²⁴⁻²⁷

In 2000 Seidel and Seppelt synthesized the first metal-xenon compound with direct gold-xenon bonds; the square planar structure of $[\text{Xe}_4\text{Au}]^{2+}$ was established by single-crystal diffraction.²⁸ Later the group reported compounds containing $[\text{Xe}_2\text{Au}]^{2+}$ and $[\text{XeAu}]^+$.²⁹⁻³⁰ Stimulated by this work, Stace and coworkers succeeded in the mass spectrometric detection of $[\text{Ar}_n\text{M}]^{2+}$ (M = Cu, Ag, Au) cluster ions in the gas phase by passing a supersonic jet of argon clusters through a vapor of noble metals followed by electron ionization.³¹ They observed $[\text{Ar}_n\text{Cu}]^{2+}$ and $[\text{Ar}_n\text{Ag}]^{2+}$ with $1 \leq n \leq 8$, and a much weaker signal of $[\text{Ar}_n\text{Au}]^{2+}$, $3 \leq n \leq 7$. Interesting features in the abundance distributions of $[\text{Ar}_n\text{Cu}]^{2+}$ and $[\text{Ar}_n\text{Ag}]^{2+}$ were maxima at $n = 4$ and sharp drops beyond $n = 6$, suggesting local anomalies in the stability of these ions. Singly charged Ar_nAu^+ ions were not mentioned in their report.³¹

Recently we reported mass spectra of helium nanodroplets doped with gold; cations containing up to 14 Au atoms and 85 of helium atoms were observed.³² With the exception of this work, there are only two other published mass spectrometric studies of singly charged noble metal ions complexed with more than two noble gas atoms: One from our lab which suggest that He_6Cu^+ , $\text{He}_{12}\text{Cu}^+$, and $\text{He}_{24}\text{Cu}^+$, are particularly stable.³³ And another one by Froudakis et al. who observed Ne_nCu^+ ($n \leq 24$) and Ar_nCu^+ ($n \leq 150$).³⁴ The abundance distributions indicated enhanced cluster ion stability at $n = 4$ and 12 for Ne_nCu^+ but at $n = 4$ and 6 for Ar_nCu^+ . These observations were consistent with electronic structure calculations that revealed that for neon the first solvation shell has icosahedral symmetry while for Ar it has octahedral symmetry.³⁴ The differences were attributed to the different values of the size ratio

$$\sigma^* = R_{\text{M-Ng}}/R_{\text{Ng-Ng}} \quad (1)$$

where $R_{\text{M-Ng}}$ is the equilibrium distance between the metal ion and the ligand while $R_{\text{Ng-Ng}}$ is the equilibrium distance between ligands. Within a hard-sphere model icosahedral packing is energetically preferred for $0.823 \leq \sigma^* \leq 0.951$ while octahedral packing is favored for $0.613 \leq \sigma^* \leq 0.707$.³⁵

Here we report mass spectra of Au^+ complexed with up to 15 He, Ne, Ar, Kr, or Xe atoms, obtained by electron ionization of helium droplets doped with gold and noble gases. Local anomalies in the ion abundances hint at particularly stable cluster sizes.³⁶ Prominent anomalies in the abundance distributions of Ar_nAu^+ , Kr_nAu^+ , and Xe_nAu^+ are local maxima at $n = 2$. The high stability of these ions is expected; it derives from the covalent character of the bond.^{1,5,10-11,37} Surprisingly, though, Ne_2Au^+ (but not He_2Au^+) forms a local abundance maximum as well. This seems to conflict with a theoretical study of Ne_nAu^+ at the CCSD(T) level which finds a higher dissociation energy for Ne_3Au^+ than for Ne_2Au^+ ,¹² and the general notion that the bonding in NeAu^+ and Ne_2Au^+ is entirely physical,^{5,11-12} i.e. the attractive forces are due entirely to the ion-induced dipole term plus other induction and dispersion attractive terms.¹¹

To the best of our knowledge, the current data present the first mass spectrometric study of solvation of a metal cation in all noble gases (ignoring radon). Thus, another aim is to establish trends in the structure and size of the solvation shell as the size ratio σ^* decreases from He to Xe. Local maxima at $\text{He}_{12}\text{Au}^+$ and $\text{Ne}_{12}\text{Au}^+$ indicate icosahedral structure, consistent with their rather large estimated values of σ^* . Ar_nAu^+ , on the other hand, seems to adopt octahedral structure, consistent with its much smaller σ^* value. A computational study of He_nAu^+ and Ar_nAu^+ , based on pairwise additive potentials computed by coupled-cluster calculations, corroborates this conclusion. Furthermore, the calculations and previously reported mass spectra³² suggest that He_nAu^+ features two additional solvation shells of I_h symmetry, similar to results obtained for other ions solvated in helium³⁸⁻³⁹ or molecular hydrogen.⁴⁰⁻⁴²

2. Experiment

Helium nanodroplets were produced by expanding helium (Messer, purity 99.9999 %) through a 5 μm nozzle, cooled by a closed-cycle refrigerator, into vacuum. The stagnation pressure and nozzle temperature varied slightly from run to run; representative values were $P_0 = 23$ bar and $T_0 = 9.6$ K.⁴³ At these conditions the droplets contain an estimated average number of 10^5 to 10^6 helium atoms.⁴⁴ The expanding beam was skimmed by a 0.8 mm conical skimmer located 8 mm downstream from the nozzle and traversed an 8 cm long, differentially pumped pick-up cell into which Ne, Ar, Kr, or Xe (Messer, research grade, partial pressure about 1×10^{-5} mbar) could be introduced. The droplet beam passed through another pick-up cell filled with gold vapor produced in a resistively heated oven. The temperature of the gold oven could not be measured, but it was varied in order to obtain the optimal conditions for formation of small Ng_nAu^+ cluster ions. He_nAu^+ ions are observed if no gas is introduced into the first pick-up cell.

The beam of doped helium droplets was collimated and crossed by an electron beam. The electron energy varied from run to run between 52 and 91 eV,⁴³ no major impact of the electron energy on the mass spectra is to be expected within this range. Cations were accelerated into the extraction region of a reflectron time-of-flight mass spectrometer (ToFwerk AG, model HTOF) with a mass resolution $m/\Delta m \approx 4500$ ($\Delta m =$ full-width-at-half-maximum). Further experimental details have been provided elsewhere.⁴⁵

3. Theory

We have generated two-body potentials for the Ng-Au^+ and Ng-Ng interactions ($\text{Ng} = \text{He}$ or Ar) based on the potential energy surfaces from *ab initio* calculations at the CCSD(T)/def2-TZVPP level. The potentials were corrected for basis set superposition error (BSSE) using the counterpoise scheme and the calculations were performed using the Gaussian 16 software.⁴⁶ Potential energy curves are displayed in Fig. S1. Classical molecular dynamics simulations of Ng_nAu^+ were run using the LAMMPS suite⁴⁷ and the potentials derived from the *ab initio* calculations were read as tabulated values.

The initial structures used in the simulations consisted of a randomized $\text{Ng}_{110}\text{Au}^+$ cluster with the Au ion located at the center. Simulations were carried out 1 K for He and 10 K for Ar for 50 ps (1 fs time step) to sample the potential energy surface of the systems and overcome barriers between different structures. At the end of each simulation, the structures were instantaneously optimized (at 0 K) to identify potential energy minima for each starting geometry. This process was repeated 100 times and the lowest potential energy structure was saved. A randomly chosen rare gas atom was then removed and the procedure was performed once again for the smaller cluster size. This was repeated for all smaller cluster sizes.

The structures of small clusters are analyzed visually while that of large clusters is analyzed by extracting their radial density distributions (rdf) in form of histograms that show the number of ligands as a function of their distance from Au^+ . Time averages from the annealing processes are also shown in the supplementary material. Results will be presented in Section 5 and the Supplemental Information.

4. Results

Fig. 1 presents a mass spectrum of helium droplets doped with gold and argon. Gold is monoisotopic (^{197}Au , mass 196.967 u); argon is nearly monoisotopic (^{40}Ar , natural abundance 99.600 %, mass 39.962 u). The most prominent mass peaks in Fig. 1a, marked by triangles, are due to bare Au_n^+ (note the logarithmic ordinate). Secondary mass peaks are due to Ar_nAu_m^+ ; they are seen more clearly in Fig. 1b which employs a linear ordinate. Mass peaks due to Ar_nAu^+ are flagged by dots and connected by a solid line. Peaks due to Ar_nAu_2^+ and Ar_nAu_3^+ are flagged by diamonds and triangles and connected by dashed lines; the first three peaks in these series are off scale.

Extracting the abundance of Ar_nAu^+ ions from the mass spectrum poses no problems because of the absence of mass spectral interference with the well resolved Ar_nAu_2^+ and Ar_nAu_3^+ series and the very weak He_n^+ series. Analyzing mass spectra of the other noble gases is more challenging because they feature two

(neon), five (krypton), or seven (xenon) naturally occurring isotopes above the 1 % level. A custom-designed software package is used to extract their ion abundance.⁴⁸ The software deconvolutes possible overlapping contributions to particular mass peaks by different ions and isotopologues. It automatically fits mass peaks, subtracts background signals, and explicitly considers isotopic patterns of all ions that are expected to contribute to a given peak.

The abundance distributions of Ng_nAu^+ ions are compiled in Fig. 2 for $\text{Ng} = \text{He}$ through Xe (panels a through e, respectively). Significant anomalies are labeled; for most data points error bars are smaller than the symbols. All noble gases except helium feature a pronounced maximum at $n = 2$. He_nAu^+ and Ne_nAu^+ feature a pronounced maximum at $n = 12$. Ar_nAu^+ is the only system that shows significant anomalies at intermediate sizes, namely at $n = 6$ and 9 .

We emphasize that these local anomalies are reproducible. For example, several abundance distributions of He_nAu^+ obtained under different experimental conditions (different helium droplet sizes and ion extraction conditions) have been presented in a previous report.³² All distributions featured a distinct local maximum at $n = 12$.

It is worth mentioning that all Ng - Au cluster ions identified in our mass spectra are singly charged. Stace and coworkers observed $\text{Ar}_n\text{Au}^{2+}$, $3 \leq n \leq 7$ by passing a supersonic beam of argon clusters through gold vapor and subsequent electron ionization of the mixed clusters at 100 eV.³¹ The researchers were solely interested in dications; they did not mention monocations in their report.

Results of our computational work will be presented and discussed in the next section; additional results will be provided as Supplemental Information.

5. Discussion

5.1 The significance of local anomalies in ion abundance distributions

The basic assumption is that, at experimental conditions prevalent in the present study, local anomalies in the abundance distribution of cluster ions Ng_nAu^+ correlate with corresponding features in their dissociation energy D_n (i.e. the energy required to adiabatically remove one noble gas atom).⁴⁹⁻⁵⁰ Cluster growth in a helium droplet by successive pick up of monomers is a statistical process which produces broad, featureless size distributions. However, subsequent electron ionization introduces a large amount of excess energy which results in fragmentation and possible enrichment of relatively stable cluster ions. For cations the process starts with the formation of He^+ in the droplet.⁵¹⁻⁵² The positive charge may jump by resonant charge exchange to an adjacent helium atom. This hopping process is terminated either by the formation of He_2^+ or by charge transfer to the dopant. In the latter case, about 15 eV (the difference between the ionization energies of helium, 24.6 eV, and gold, 9.2 eV) will be released.⁵²⁻⁵³ This energy exceeds the evaporation energy of bulk helium by a factor 24000.

The large excess energy leads to cluster ion ejection from the helium droplet and extensive fragmentation. Milliseconds elapse between ionization and mass analysis, providing ample time for the ions to cool by evaporation, enriching stable ions and depleting unstable ions. The relation between cluster abundance measured by mass spectrometry and (relative) dissociation energy is intricate.⁵⁴⁻⁵⁵ The relation becomes semiquantitative for cluster ions whose heat capacity is much less than the classical value;³⁶ a comparison of measured ion abundances with calculated dissociation energies for $\text{He}_n\text{C}_{60}^+$ ⁵⁶ and He_nAr^+ ³⁸⁻³⁹ supports that conclusion. The relation will be more complex for systems whose vibrational degrees of freedom are not frozen out as easily.⁵⁷ Qualitatively, however, it is clear that an abrupt decrease of the dissociation energy (i.e. $D_{n+1} \ll D_n$) will cause an enrichment of cluster ion A_n^+ at the expense of A_{n+1}^+ . There are several different scenarios, such as a single cluster size that is particularly stable (a “magic” cluster) or particularly unstable with respect to its neighbors, or closure of a solvation shell where D_n drops in a stepwise fashion. For simplicity we merely assume that a local maximum or abrupt drop in the ion abundance at a magic number n indicates that the dissociation energy of A_n^+ is considerably larger than that of A_{n+1}^+ .

Note that dissociation energies refer to zero temperature, i.e. they measure the energy difference between ground state structures. Evaporations, however, require finite temperatures, and one should really speak of free energies which may involve significant contributions from configurational entropies.⁵⁸ Entropic contributions are commonly neglected primarily because it is challenging to quantitatively account for them.

5.2 Magic numbers at $n = 2$

The abundance distributions of Ne_nAu^+ , Ar_nAu^+ , Kr_nAu^+ , and Xe_nAu^+ feature a local maximum at $n = 2$, suggesting that the dissociation energy of Ng_2Au^+ greatly exceeds that of Ng_3Au^+ . The abundance of He_2Au^+ , on the other hand, is not enhanced. Are these results consistent with previous work?

Early research was focused on XeAu^+ , the most stable of the diatomic ions. Pyykkö applied the CCSD(T) method and obtained a dissociation energy of $D_e = 0.91$ eV.¹ Other values obtained with CCSD(T) and various basis sets are 1.31 eV,⁷ 1.248 eV,⁹ 1.33 eV,¹⁰ 1.305 eV,¹¹ and 1.104 eV.⁵⁹ Electron correlation and relativistic effects have strong influence on the geometries and stabilities; they shorten the bond length and enhance the stability by some 50 %.^{1,60}

Some studies have been devoted to diatomics containing noble gases lighter than Xe. Partly filled symbols in Fig. 3 represent D_e values obtained by Yousef et al. with the RCCSD(T) procedure.⁹ Several other theoretical groups have investigated these diatomics.^{1,10-11,16-17} Their results are not included in Fig. 3 but they agree with Yousef's results within better than 10 %. The only exception are early results by Pyykkö¹ that were about 25 to 45 % below those of Yousef et al.⁹

A few theoretical studies have been devoted to triatomic Ng_2Au^+ ,^{1,5} but for a discussion of the magic number at $n = 2$ one needs dissociation energies that extend to $n = 3$ or larger. The only such data have been calculated by Li et al. for Ne through Xe ($n \leq 3$) at the CCSD(T) level^{12,37,59,61} and by Zhang et al. for Ar ($n \leq 6$) at the B3LYP level.⁶² Their results are displayed in Fig. 3 by solid symbols connected by lines.

Fig. 3 reveals two striking features:

1. The stability of NgAu^+ and Ng_2Au^+ increases from He to Xe. The increase is less than a factor 2 from Ar to Kr to Xe, but much stronger (factor 7) from Ne to Ar.
2. For Ar, Kr and Xe the dissociation energy of Ng_2Au^+ is slightly larger than that of NgAu^+ but much larger (factor 2) than that of Ng_3Au^+ . In contrast, the dissociation energy of Ne_2Au^+ is slightly weaker than that of its neighbors.⁶³

Feature (1) reflects the notion that the bond in NgAu^+ and Ng_2Au^+ has significant covalent character for Xe and Kr, a slight covalent contribution for Ar,^{1,5,10-11,37} but no covalent character for Ne.^{5,11-12} However, as pointed out by Yousef et al.,⁹ the large jump in the static electric dipole polarizability between Ne (0.396 \AA^3) and Ar (1.64 \AA^3) is the main reason for the strong increase in stability from NeAu^+ to ArAu^+ .

Feature (2) poses a conundrum: Ne_2Au^+ forms a distinct local maximum in the ion abundance, similar to that of Ar_2Au^+ and the heavier noble gases, but its computed dissociation energy is not enhanced relative to that of Ne_3Au^+ .¹² This suggests that theory underestimates the stability of Ne_2Au^+ or overestimates that of Ne_3Au^+ .

It is tempting to conclude that the bond in NeAu^+ and Ne_2Au^+ is not entirely physical, contrary to conclusions drawn in previous studies.^{5,11-12} A comparison with alkali ions solvated in noble gases, which are model systems for purely physical bonding, is instructive. For example, the structure and stability of alkali ions (Li^+ , Na^+ , K^+ and Cs^+) solvated in xenon has been explored by different theoretical approaches.⁶⁴⁻⁶⁷ The calculated dissociation energies do not feature enhanced binding at $n = 2$, even if pairwise additive potentials are augmented by three-body contributions that account for the interaction between the dipoles induced by the ion on the noble gas atoms.

5.3 The geometrical structure of He_nAu^+ , Ne_nAu^+ , and Ar_nAu^+

The abundance distributions in Fig. 2 feature magic numbers beyond $n = 2$, most noticeably at $n = 12$ for helium and neon, and $n = 6, 9$ for argon. What information do these numbers convey? In general, magic numbers may be used to qualitatively test structural models if the proposed structure lends enhanced stability to particular sizes. For Au^+ solvated in He, Ne and Ar, the interaction is predominantly physical⁵ and the interaction is reasonably well described by pairwise additive potentials. In this situation, the dissociation energy will feature an abrupt drop beyond the first coordination shell (closure of secondary shells, or partial closure of a shell, may give rise to additional anomalies). Hence, the magic number will count the number of ligands in the first solvation shell (from here on called n_1) and reflect, indirectly, its geometric structure.

In the simplest approximation, n_1 merely depends on the size of the ion relative to that of the ligand. It is convenient to characterize these two quantities by the size ratio $\sigma^* = R_{\text{M-Ng}}/R_{\text{Ng-Ng}}$ (see eq. 1). σ^* slightly below 1 will favor icosahedral arrangements; structures with smaller coordination numbers such as a square antiprism (a twisted cube, symmetry D_{4h}), octahedron (O_h), or tetrahedron (T_d) will be preferred as the value of σ^* decreases.⁶⁷ Prekas et al. have calculated, within a hard-sphere model, the values of σ^* at which structural transitions occur.³⁵ Their results are summarized in Fig. 4 below the abscissa. For example, the solvated ion will fit tightly into an octahedral shell ($n_1 = 6$) if $\sigma^* = 0.707$. The shell can no longer accommodate the ion if $\sigma^* > 0.707$, the ligands will no longer be in direct contact with each other, and the shell converts to a square antiprism ($n_1 = 8$) which offers a larger cavity.⁶⁸ The square antiprism can no longer accommodate the ion when σ^* exceeds 0.823 and the ligands adopt icosahedral structure ($n_1 = 12$). The icosahedral shell will rupture if σ^* exceeds 0.951 and a close-packed (crystalline face centered or hexagonal) structure will be favorable.

Prekas et al. have tested the predictions of the hard-sphere model with molecular dynamics simulations in which the ligand-ligand as well as the ion-ligand interactions were modeled by Lennard Jones potentials and the value of σ^* was varied systematically.³⁵ The basic features of the hard-sphere model were confirmed but the structure of incomplete solvation shells was found to also depend on the cluster size.^{35,69}

These trends have been confirmed in various experimental studies, for example for Na^+ , Al^+ , and In^+ ,⁷⁰ for K^+ and Mg^+ ,³⁵ Li^+ ,⁷¹ and Cu^+ ³⁴ solvated in various noble gases. Support also comes from theoretical studies employing more realistic two- or three-body potentials for the ion-ligand and ligand-ligand interactions; for example, for different alkali ions solvated in xenon⁶⁴⁻⁶⁷.

We adopt these ideas in order to “predict” the structure and size of the first solvation shell in Ng_nAu^+ . We equate $R_{\text{M-Ng}}$ with the equilibrium distance in NgAu^+ calculated by Yousef et al. for $\text{Ng} = \text{He}$,⁹ and by Breckenridge et al. for Ne through Xe.¹¹ $R_{\text{Ng-Ng}}$ is equated with the nearest-neighbor distance in noble-gas crystals which adopt close-packed structures.⁷² For Ne through Xe these crystal values deviate less than 3 % from the well-known equilibrium distance of the diatomics; for He this choice avoids bias arising from the exceedingly large zero-point motion in He_2 .⁷³

The values of σ^* thus obtained are indicated in Fig. 4 above the abscissa. Based on this simple model one would expect an icosahedral (or close-packed) structure for the first solvation shell in He_nAu^+ and Ne_nAu^+ , i.e. closure of the first solvation shell at $n_1 = 12$. For Ar_nAu^+ one would expect an octahedral solvation shell ($n_1 = 6$). These features agree with the anomalies observed in the ion abundance, Fig. 2.

Thus, a simple hard-sphere model³⁵ provides a rational for the anomalies observed in the abundance distributions of Au^+ solvated in He, Ne, and Ar. We discard the predictions of Fig. 4 for Kr_nAu^+ and Xe_nAu^+ because the presence of strong covalent bonding is inconsistent with the assumption of non-directional bonding.

For further insight we have performed molecular dynamics simulations of He_nAu^+ and Ar_nAu^+ assuming two-body ion-ligand and ligand-ligand interaction. The dissociation energies computed for small Ar_nAu^+ (not corrected for zero point energy) are displayed in Fig. 5b; results for He_nAu^+ are provided in the Supplemental Information, Fig. S4. Also included are results obtained by Zhang et al. at the B3LYP level for $n \leq 6$.⁶² Our Ar_nAu^+ data indicate enhanced binding for $n = 6$ and 9, in agreement with the local anomalies in the abundance distributions (Fig. 5a). We emphasize, however, that our simulations do not account for covalent bonding; they cannot correctly predict the structure and energy of the ionic core; they cannot reproduce the anomaly at $n = 2$. Ar_6Au^+ has octahedral structure, in agreement with the B3LYP calculation by Zhang et al.. Ar_7Au^+ is a capped octahedron but Ar_8Au^+ converts to the square antiprism. The structures of the magic Ar_9Au^+ and $\text{Ar}_{10}\text{Au}^+$ vaguely resemble those of a capped and bicapped square antiprism, respectively. Geometries of select ions are displayed in the Supplemental Information (Fig. S5).

A convenient way to identify the presence and size of solvation shells is provided by radial density functions which are obtained by plotting the number of atoms versus their distance from the solvated ion. The histograms in Fig. 6 (red lines) represent rdfs of $\text{He}_{110}\text{Au}^+$ and $\text{Ar}_{108}\text{Au}^+$ at the end of a simulation, i.e. at 0 K (panels a and b, respectively). They reveal several distinct solvation shells. In order to determine the number of atoms in the shells we evaluate the cumulative number of atoms in the histograms *versus* distance, resulting in the blue curves.

For Ar (Fig. 6b), the total number of atoms within the first, first two, first three, and first four shells are 6, 10, 22 and 34, respectively. The number 10 does not quite agree with the anomaly at 9 that we identified in the plot of dissociation energies and ion abundances (Fig. 5). There are two possible reasons for this disagreement: i) The simulation of $\text{Ar}_{108}\text{Au}^+$ may have failed to produce the minimum energy structure. ii) The coordination number n_1 may slightly increase with cluster size because atoms in outer shells will exert additional forces on the atoms in the first shell.⁷⁴

In contrast, the dissociation energy D_n is determined from simulations of much smaller clusters (D_9 , e.g., equals the difference between the total energies of $\text{Ar} + \text{Ar}_8\text{Au}^+$ and Ar_9Au^+). In the Supplement (Fig. S3) we show the rdf of $\text{Ar}_{108}\text{Au}^+$ averaged over the full (50 ps) duration of the simulation at 10 K. Peaks are broader, the third and higher peaks are no longer distinct, and the cumulative sum of atoms in the first two shells equals 9, consistent with the computed dissociation energies.

For He, the total number of atoms within the first, first two and first three shells are 12, 32, and 44, respectively. Abundance distributions of He_nAu^+ extending to $n = 85$ have been presented in a previous publication.³² They do reveal, indeed, small but statistically significant abrupt drops on an otherwise smooth distribution at $n = 32$ and 44, in addition to the strong anomaly at 12. This same set of magic numbers (12, 32, 44) was more readily discernible in the ion abundance of Ar^+ solvated in He,³⁸ and Cs^+ or H^+ solvated in molecular hydrogen.⁴⁰⁻⁴¹ Theoretical studies of He_nAr^+ employing the Path Integral Monte Carlo method³⁹ and of $(\text{H}_2)_n\text{H}^+$ using CCSD(T)⁴² reveal that these magic numbers reflect successive closure of three concentric

solvation shells in which the ligands are placed at the vertices of platonic solids, namely an icosahedron, a dodecahedron, and an icosahedron.

Whereas the number of atoms in a solvation shell can be reliably surmised from the rdf, a structural characterization becomes challenging if the interaction between the ion and the ligands is weak and quantum effects dominate, as demonstrated in a recent study of Cs⁺ solvated in helium.⁷⁵ In this system the Lindeman index which measures the root-mean-square bond length fluctuation indicates a fluid-like solvation shell. On the other hand, the first three helium layers around the smaller, more strongly bound Ar⁺ appear to form a highly ordered solid.³⁹ The estimated ion-ligand distance of He-Au⁺ ($R_{M-Ng} = 2.44 \text{ \AA}$) is even shorter than that of He-Ar⁺ (2.57 Å),⁹ suggesting⁷⁵ that the interaction in He_nAu⁺ is even stronger than in He_nAr⁺, thus favoring solid-like order in He_nAu⁺. It is also interesting to note that the first three peaks in the time-averaged rdf of He_nAu⁺ (see Fig S2) remain distinct.

Conclusion

We have measured ion abundance distributions of Au⁺ solvated in all noble gases, helium through xenon. Local maxima in the ion abundance for Ar₂Au⁺, Kr₂Au⁺, Xe₂Au⁺ suggest that their dissociation energies are much larger than those of the corresponding Ng₃Au⁺, in agreement with the covalent character of bonding in these systems.^{1,5,10-11} and calculated dissociation energies.^{12,37,59,61-62} Surprisingly, though, Ne₂Au⁺ features an enhanced abundance as well, contrary to the notion that its bond is entirely physical and its dissociation energy is below that of Ne₃Au⁺.^{5,11-12} Anomalies in the ion abundance of He_nAu⁺ and Ne_nAu⁺ at $n = 12$ and Ar_nAu⁺ at 6 can be assigned to icosahedral and octahedral solvation shells, consistent with the relative size of the solvated ions. Model calculations with pairwise additive potentials provide further insight into the structure of these cluster ions. They suggest two additional solvation shells of icosahedral symmetry in He_nAu⁺, consistent with weak but statistically significant features in the abundance distributions. Structural order in helium snowballs beyond the first solvation shell is the exception rather than the rule;⁷⁴ for a complete discussion one will have to consider not only the size ratio σ^* and the strength of the ion-ligand interaction but the shape of the ion-ligand interaction potential as well.³⁹

Supplemental Information

Shown are potential energy curves of the ion-ligand and ligand-ligand interaction, radial density functions, dissociation energies, and geometric structures of select sizes of He_nAu⁺ and Ar_nAu⁺.

Acknowledgement

This work was supported by the Austrian Science Fund, FWF (Projects I4130, P31149, and W1259), the Swedish Research Council (contract No. 2016-06625), and the European Commission (ELEvaTE H2020 Twinning Project, Project No. 692335).

References

1. Pyykkö, P. Predicted Chemical Bonds between Rare Gases and Au⁺. *J. Am. Chem. Soc.* **1995**, *117*, 2067-2070.
2. Read, J. P.; Buckingham, A. D. Covalency in ArAu⁺ and Related Species? *J. Am. Chem. Soc.* **1997**, *119*, 9010-9013.
3. Zeng, T.; Klobukowski, M. Relativistic Model Core Potential Study of the Au⁺Xe System. *J. Phys. Chem. A* **2008**, *112*, 5236-5242.
4. Jamshidi, Z.; Eskandari, K.; Azami, S. M. Nature of Closed- and Open-Shell Interactions between Noble Metals and Rare Gas Atoms. *Int. J. Quantum Chem.* **2013**, *113*, 1981-1991.
5. Grabowski, S. J.; Ugalde, J. M.; Andrada, D. M.; Frenking, G. Comparison of Hydrogen and Gold Bonding in [XHX]⁻, [XAuX]⁻ and Isoelectronic [NgHNg]⁺, [NgAuNg]⁺ (X=Halogen, Ng=Noble Gas). *Chem. - Eur. J.* **2016**, *22*, 11317-11328.
6. Zou, W. L.; Nori-Shargh, D.; Boggs, J. E. On the Covalent Character of Rare Gas Bonding Interactions: A New Kind of Weak Interaction. *J. Phys. Chem. A* **2013**, *117*, 207-212.
7. Schröder, D.; Schwarz, H.; Hrusak, J.; Pyykkö, P. Cationic Gold(I) Complexes of Xenon and of Ligands Containing the Donor Atoms Oxygen, Nitrogen, Phosphorus, and Sulfur. *Inorg. Chem.* **1998**, *37*, 624-632.
8. Bellert, D.; Breckenridge, W. H. Bonding in Ground-State and Excited-State A⁺Rg van der Waals Ions (A = Atom, Rg = Rare-Gas Atom): A Model-Potential Analysis. *Chem. Rev.* **2002**, *102*, 1595-1622.

9. Yousef, A.; Shrestha, S.; Viehland, L. A.; Lee, E. P. F.; Gray, B. R.; Ayles, V. L.; Wright, T. G.; Breckenridge, W. H. Interaction Potentials and Transport Properties of Coinage Metal Cations in Rare Gases. *J. Chem. Phys.* **2007**, *127*, 154309.
10. Belpassi, L.; Infante, I.; Tarantelli, F.; Visscher, L. The Chemical Bond between Au(I) and the Noble Gases. Comparative Study of NgAuF and NgAu⁺ (Ng = Ar, Kr, Xe) by Density Functional and Coupled Cluster Methods. *J. Am. Chem. Soc.* **2008**, *130*, 1048-1060.
11. Breckenridge, W. H.; Ayles, V. L.; Wright, T. G. Evidence for Emergent Chemical Bonding in Au⁺-Rg Complexes (Rg = Ne, Ar, Kr, and Xe). *J. Phys. Chem. A* **2008**, *112*, 4209-4214.
12. Li, X. Y.; Zhou, C. F.; Cao, X.; Zhao, Y. F. Theoretical Investigation of Stabilities and Interactions of AuNe_n^Z (n = 1-3, Z = -1,0,+1) Clusters. *Mol. Phys.* **2009**, *107*, 2531-2536.
13. Plowright, R. J.; Gardner, A. M.; Withers, C. D.; Wright, T. G.; Morse, M. D.; Breckenridge, W. H. Electronic Spectroscopy of the 6p ← 6s Transition in Au-Ne: Trends in the Au-RG Series. *J. Phys. Chem. A* **2010**, *114*, 3103-3113.
14. Gardner, A. M.; Plowright, R. J.; Watkins, M. J.; Wright, T. G.; Breckenridge, W. H. Theoretical Study of the X²Σ⁺ States of the Neutral CM-RG Complexes (CM = Coinage Metal, Cu, Ag, and Au and RG = Rare Gas, He-Rn). *J. Chem. Phys.* **2010**, *132*, 184301.
15. Lai, T. Y.; Yang, C. Y.; Lin, H. J.; Yang, C. Y.; Hu, W. P. Benchmark of Density Functional Theory Methods on the Prediction of Bond Energies and Bond Distances of Noble-Gas Containing Molecules. *J. Chem. Phys.* **2011**, *134*, 244110.
16. Tong, X. F.; Yang, C. L.; Wang, M. S.; Ma, X. G.; Wang, D. H. Interactions of M^z-X Complexes (M = Cu, Ag, and Au; X = He, Ne, and Ar; and z = ±1). *J. Chem. Phys.* **2011**, *134*, 024306.
17. Viehland, L. A.; Yang, C. L. Improved Techniques for the Calculation of Ab Initio Ion-Neutral Interaction Potentials: Application to Coinage Metal Ions Interacting with Rare Gas Atoms. *Mol. Phys.* **2015**, *113*, 3874-3882.
18. Pan, S.; Jana, G.; Merino, G.; Chattaraj, P. K. Noble-Noble Strong Union: Gold at Its Best to Make a Bond with a Noble Gas Atom. *ChemistryOpen* **2019**, *8*, 173-187.
19. Kapur, S.; Müller, E. W. Metal-Neon Compound Ions in Slow Field Evaporation. *Surf. Sci.* **1977**, *62*, 610-620.
20. Hopkins, W. S.; Woodham, A. P.; Plowright, R. J.; Wright, T. G.; Mackenzie, S. R. A Velocity Map Imaging Study of Gold-Rare Gas Complexes: Au-Ar, Au-Kr, and Au-Xe. *J. Chem. Phys.* **2010**, *132*, 214303.
21. Gao, Y.; Huang, W.; Woodford, J.; Wang, L. S.; Zeng, X. C. Detecting Weak Interactions between Au- and Gas Molecules: A Photoelectron Spectroscopic and Ab Initio Study. *J. Am. Chem. Soc.* **2009**, *131*, 9484-9485.
22. Ghiringhelli, L. M.; Gruene, P.; Lyon, J. T.; Rayner, D. M.; Meijer, G.; Fielicke, A.; Scheffler, M. Not So Loosely Bound Rare Gas Atoms: Finite-Temperature Vibrational Fingerprints of Neutral Gold-Cluster Complexes. *New J. Phys.* **2013**, *15*, 083003.
23. Shayeghi, A.; Johnston, R. L.; Rayner, D. M.; Schäfer, R.; Fielicke, A. The Nature of Bonding between Argon and Mixed Gold-Silver Trimers. *Angew. Chem. Int. Ed.* **2015**, *54*, 10675-10680.
24. Jamshidi, Z.; Far, M. F.; Maghari, A. Binding of Noble Metal Clusters with Rare Gas Atoms: Theoretical Investigation. *J. Phys. Chem. A* **2012**, *116*, 12510-12517.
25. Mancera, L. A.; Benoit, D. M. The Nature and Role of the Gold-Krypton Interactions in Small Neutral Gold Clusters. *J. Phys. Chem. A* **2015**, *119*, 3075-3088.
26. Ghiringhelli, L. M.; Levchenko, S. V. Strengthening Gold-Gold Bonds by Complexing Gold Clusters with Noble Gases. *Inorg. Chem. Comm.* **2015**, *55*, 153-156.
27. Ghosh, A.; Ghanty, T. K. Unprecedented Enhancement of Noble Gas-Noble Metal Bonding in NgAu₃⁺ (Ng = Ar, Kr, and Xe) Ion through Hydrogen Doping. *J. Phys. Chem. A* **2016**, *120*, 9998-10006.
28. Seidel, S.; Seppelt, K. Xenon as a Complex Ligand: The Tetra Xenono Gold(II) Cation in AuXe₄²⁺(Sb₂F₁₁)₂. *Science* **2000**, *290*, 117-118.
29. Drews, T.; Seidel, S.; Seppelt, K. Gold - Xenon Complexes. *Angew. Chem. Int. Ed.* **2002**, *41*, 454-456.
30. Hwang, I. C.; Seidel, S.; Seppelt, K. Gold(I) and Mercury(II) Xenon Complexes. *Angew. Chem. Int. Ed.* **2003**, *42*, 4392-4395.
31. Walker, N. R.; Wright, R. R.; Barran, P. E.; Cox, H.; Stace, A. J. Unexpected Stability of [CuAr]²⁺, [AgAr]²⁺, [AuAr]²⁺, and Their Larger Clusters. *J. Chem. Phys.* **2001**, *114*, 5562-5567.
32. Goulart, M.; Gatchell, M.; Kranabetter, L.; Kuhn, M.; Martini, P.; Gitzl, N.; Rainer, M.; Postler, J.; Scheier, P.; Ellis, A. M. The Adsorption of Helium Atoms on Small Cationic Gold Clusters. *Phys. Chem. Chem. Phys.* **2018**, *20*, 9554-9560.

33. Raggl, S.; Gitzl, N.; Martini, P.; Scheier, P.; Echt, O. Helium Nanodroplets Doped with Copper and Water. *Eur. Phys. J. D* **2018**, *72*, 130.
34. Froudakis, G. E.; Muhlhauser, M.; Farantos, S. C.; Sfounis, A.; Velegrakis, M. Mass Spectra and Structures of Cu^+Rg_n Clusters ($\text{Rg} = \text{Ne, Ar}$). *Chem. Phys.* **2002**, *280*, 43-51.
35. Prekas, D.; Lüder, C.; Velegrakis, M. Structural Transitions in Metal Ion-Doped Noble Gas Clusters: Experiments and Molecular Dynamics Simulations. *J. Chem. Phys.* **1998**, *108*, 4450-4459.
36. An der Lan, L.; Bartl, P.; Leidlmair, C.; Jochum, R.; Denifl, S.; Echt, O.; Scheier, P. Solvation of Na^+ , K^+ and Their Dimers in Helium. *Chem. - Eur. J.* **2012**, *18*, 4411-4418.
37. Li, X. Y.; Cao, X.; Zhao, Y. F. Ab Initio Study of MAr_n^+ ($\text{M} = \text{Cu, Ag, and Au, } n = 1-3$). *J. Phys. B* **2009**, *42*, 065102.
38. Bartl, P.; Leidlmair, C.; Denifl, S.; Scheier, P.; Echt, O. On the Size and Structure of Helium Snowballs Formed around Charged Atoms and Clusters of Noble Gases. *J. Phys. Chem. A* **2014**, *118*, 8050–8059.
39. Tramonto, F.; Salvestrini, P.; Nava, M.; Galli, D. E. Path Integral Monte Carlo Study Confirms a Highly Ordered Snowball in ^4He Nanodroplets Doped with an Ar^+ Ion. *J. Low Temp. Phys.* **2015**, *180*, 29–36.
40. Kranabetter, L.; Goulart, M.; Aleem, A.; Kurzthaler, T.; Kuhn, M.; Barwa, E.; Renzler, M.; Scheier, P.; Echt, O. Cs^+ Solvated in Hydrogen – Evidence for Several Distinct Solvation Shells. *J. Phys. Chem. C* **2017**, *121*, 10887–10892.
41. Renzler, M.; Kuhn, M.; Mauracher, A.; Lindinger, A.; Scheier, P.; Ellis, A. M. Anionic Hydrogen Cluster Ions as a New Form of Condensed Hydrogen. *Phys. Rev. Lett.* **2016**, *117*, 273001.
42. Joshi, M.; Ghosh, A.; Ghanty, T. K. Atom- and Ion-Centered Icosahedral Shaped Subnanometer-Sized Clusters of Molecular Hydrogen. *J. Phys. Chem. C* **2017**, *121*, 15036-15048.
43. The expansion conditions were (P_0/bar , T_0/K) = (22.5, 9.4) for undoped helium droplets, and (22, 9.7), (21, 9.8), (24, 9.5), and (22, 9.65) for droplets subsequently doped with neon, argon, krypton and xenon, respectively. The energy of the ionizing electrons was 55 eV for undoped droplets, and 57, 52, 91, and 64 eV for droplets doped with Ne, Ar, Kr, Xe, respectively.
44. Gomez, L. F.; Loginov, E.; Sliter, R.; Vilesov, A. F. Sizes of Large He Droplets. *J. Chem. Phys.* **2011**, *135*, 154201.
45. Schöbel, H.; Bartl, P.; Leidlmair, C.; Denifl, S.; Echt, O.; Märk, T. D.; Scheier, P. High-Resolution Mass Spectrometric Study of Pure Helium Droplets, and Droplets Doped with Krypton. *Eur. Phys. J. D* **2011**, *63*, 209-214.
46. Frisch, M. J.; Trucks, G. W.; Schlegel, H. B.; Scuseria, G. E.; Robb, M. A.; Cheeseman, J. R.; Scalmani, G.; Barone, V.; Petersson, G. A.; Nakatsuji, H.; et al. *Gaussian 16 Rev. A.03*, Wallingford, CT, 2016.
47. Plimpton, S. Fast Parallel Algorithms for Short-Range Molecular Dynamics. *J. Comput. Phys.* **1995**, *117*, 1-19.
48. Ralser, S.; Postler, J.; Harnisch, M.; Ellis, A. M.; Scheier, P. Extracting Cluster Distributions from Mass Spectra: IsotopeFit. *Int. J. Mass Spectrom.* **2015**, *379*, 194-199.
49. Klots, C. E. Evaporation from Small Particles. *J. Phys. Chem.* **1988**, *92*, 5864-5868.
50. Hansen, K.; Näher, U. Evaporation and Cluster Abundance Spectra. *Phys. Rev. A* **1999**, *60*, 1240-1250.
51. Ellis, A. M.; Yang, S. F. Model for the Charge-Transfer Probability in Helium Nanodroplets Following Electron-Impact Ionization. *Phys. Rev. A* **2007**, *76*, 032714.
52. Mauracher, A.; Echt, O.; Ellis, A. M.; Yang, S.; Bohme, D. K.; Postler, J.; Kaiser, A.; Denifl, S.; Scheier, P. Cold Physics and Chemistry: Collisions, Ionization and Reactions inside Helium Nanodroplets Close to Zero K. *Phys. Rep.* **2018**, *751*, 1-90.
53. Mauracher, A.; Daxner, M.; Huber, S. E.; Postler, J.; Renzler, M.; Denifl, S.; Scheier, P.; Ellis, A. M. The Interaction of He^- with Fullerenes. *J. Chem. Phys.* **2015**, *142*, 104306.
54. Casero, R.; Soler, J. M. Onset and Evolution of "Magic Numbers" in Mass Spectra of Molecular Clusters. *J. Chem. Phys.* **1991**, *95*, 2927-2935.
55. Hansen, K. *Statistical Physics of Nanoparticles in the Gas Phase*. Springer Series on Atomic, Optical, and Plasma Physics Vol. 73, 2nd edition, 2019.
56. Leidlmair, C.; Wang, Y.; Bartl, P.; Schöbel, H.; Denifl, S.; Probst, M.; Alcamí, M.; Martín, F.; Zettergren, H.; Hansen, K.; et al. Structures, Energetics and Dynamics of Helium Adsorbed on Isolated Fullerene Ions. *Phys. Rev. Lett.* **2012**, *108*, 076101.
57. Hansen, K.; Andersson, P. U.; Uggerud, E. Activation Energies for Evaporation from Protonated and Deprotonated Water Clusters from Mass Spectra. *J. Chem. Phys.* **2009**, *131*, 124303.

58. Prasalovich, S.; Hansen, K.; Kjellberg, M.; Popok, V. N.; Campbell, E. E. B. Surface Entropy of Rare-Gas Clusters. *J. Chem. Phys.* **2005**, *123*, 084317.
59. Li, X. Y.; Cao, X.; Zhao, Y. F. Structure and Stability of AuXe_n^Z ($n = 1-3$, $Z = -1, 0, +1$) Clusters. *Theor. Chem. Acc.* **2009**, *123*, 469-475.
60. Li, X. Y.; Cao, X. Ab Initio Study of MXe_n^+ ($M = \text{Cu, Ag, and Au}$; $n = 1, 2$). *Phys. Rev. A* **2008**, *77*, 022508.
61. Li, X. Y.; Cao, X.; Zhao, Y. F. Interactions of MKr_n^+ ($M = \text{Cu, Ag, and Au}$; $n = 1-3$): Ab Initio Calculations. *Aust. J. Chem.* **2009**, *62*, 121-125.
62. Zhang, P. X.; Zhao, Y. F.; Hao, F. Y.; Song, X. D.; Zhang, G. H.; Wang, Y. Structures and Stabilities of Au^+Ar_n ($n = 1-6$) Clusters. *J. Mol. Struct. (Theochem)* **2009**, *899*, 111-116.
63. A study by Grabowski et al.⁵ at the CCSD(T)/aug-cc-pVTZ level confirms some of these trends. The authors reported total (i.e. atomization) energies for Ng_2Au^+ but not for NgAu^+ . If one adopts energies obtained by Yousef et al.⁹ for NgAu^+ one finds that the dissociation energies of triatomics are slightly larger than those of diatomics for Ar, Kr, Xe, but about 30 % smaller for Ne.
64. Al-Ahmari, M.; Saidi, S.; Dhiflaoui, J.; Hassen, F.; Berriche, H. Structure and Stability of the Li^+Xe_n and LiXe_n Clusters. *J. Cluster Sci.* **2015**, *26*, 913-924.
65. Slama, M.; Issa, K.; Ben Mohamed, F. E.; Rhouma, M. B.; Spiegelman, F. Structure and Stability of Na^+Xe_n Clusters. *Eur. Phys. J. D* **2016**, *70*, 242.
66. Slama, M.; Issa, K.; Zbidi, M.; Rhouma, M. B. Microsolvation of K^+ in Xenon Clusters: A Three-Body Approximation and Structural Transition. *Mol. Phys.* **2017**, *115*, 757-770.
67. Hernandez-Rojas, J.; Wales, D. J. Global Minima for Rare Gas Clusters Containing One Alkali Metal Ion. *J. Chem. Phys.* **2003**, *119*, 7800-7804.
68. Two atoms may be added to the square antiprism to form the closed-shell bicapped antiprism ($n_1 = 10$),³⁵ but the distance of the caps from the ion will exceed $R_{\text{M-Ng}}$.
69. Generally speaking, icosahedral structures will reappear as the size of the cluster grows well beyond the first solvation shell even if σ^* is rather small.^{65,67}
70. Lüder, C.; Prekas, D.; Velegakis, M. Ion-Size Effects in the Growth Sequences of Metal-Ion-Doped Noble Gas Clusters. *Laser Chem.* **1997**, *17*, 109-122.
71. Froudakis, G. E.; Farantos, S. C.; Velegakis, M. Mass Spectra and Theoretical Modeling of Li^+Ne_n , Li^+Ar_n and Li^+Kr_n Clusters. *Chem. Phys.* **2000**, *258*, 13-20.
72. Kittel, C. *Introduction to Solid State Physics*. 8 ed.; John Wiley & Sons: New York, 2004.
73. Grisenti, R. E.; Schöllkopf, W.; Toennies, J. P.; Hegerfeldt, G. C.; Köhler, T.; Stoll, M. Determination of the Bond Length and Binding Energy of the Helium Dimer by Diffraction from a Transmission Grating. *Phys. Rev. Lett.* **2000**, *85*, 2284.
74. Galli, D. E.; Ceperley, D. M.; Reatto, L. Path Integral Monte Carlo Study of ^4He Clusters Doped with Alkali and Alkali-Earth Ions. *J. Phys. Chem. A* **2011**, *115*, 7300-7309.
75. de Tudela, R. P.; Martini, P.; Goulart, M.; Scheier, P.; Pirani, F.; Hernandez-Rojas, J.; Breton, J.; de Zarate, J. O.; Bartolomei, M.; Gonzalez-Lezana, T.; et al. A Combined Experimental and Theoretical Investigation of Cs^+ Ions Solvated in He_n Clusters. *J. Chem. Phys.* **2019**, *150*, 154304.

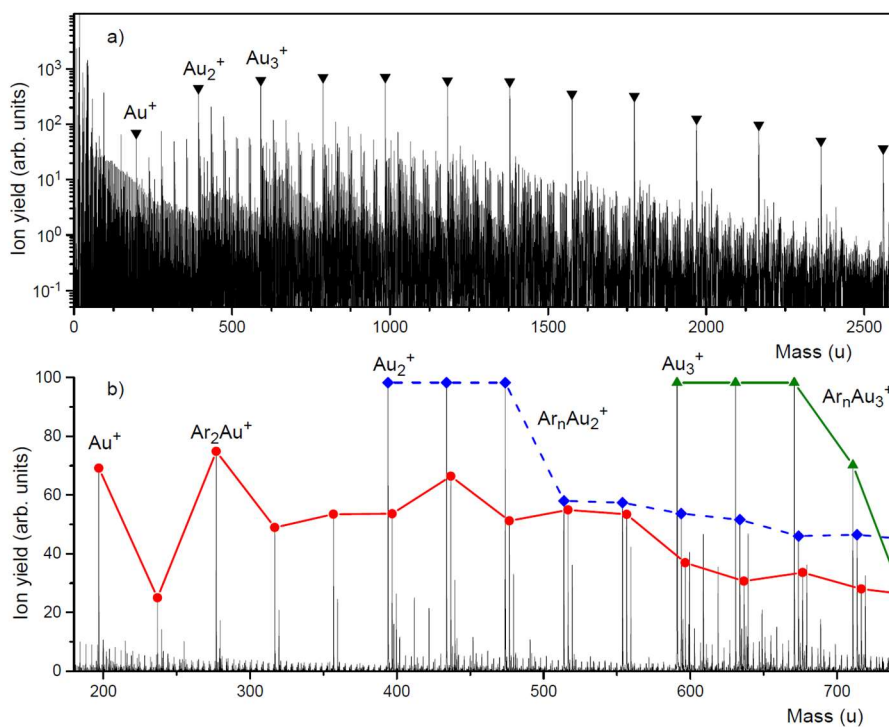


Fig. 1. Panel a: Mass spectrum of helium nanodroplets doped with gold and argon. Mass peaks due to bare Au_m^+ , $1 \leq m \leq 13$, are marked. Panel b shows a section of the mass spectrum plotted with a linear ordinate. Ion series due to Ar_nAu^+ , $Ar_nAu_2^+$, and $Ar_nAu_3^+$ are marked by dots, diamonds, and triangles, respectively.

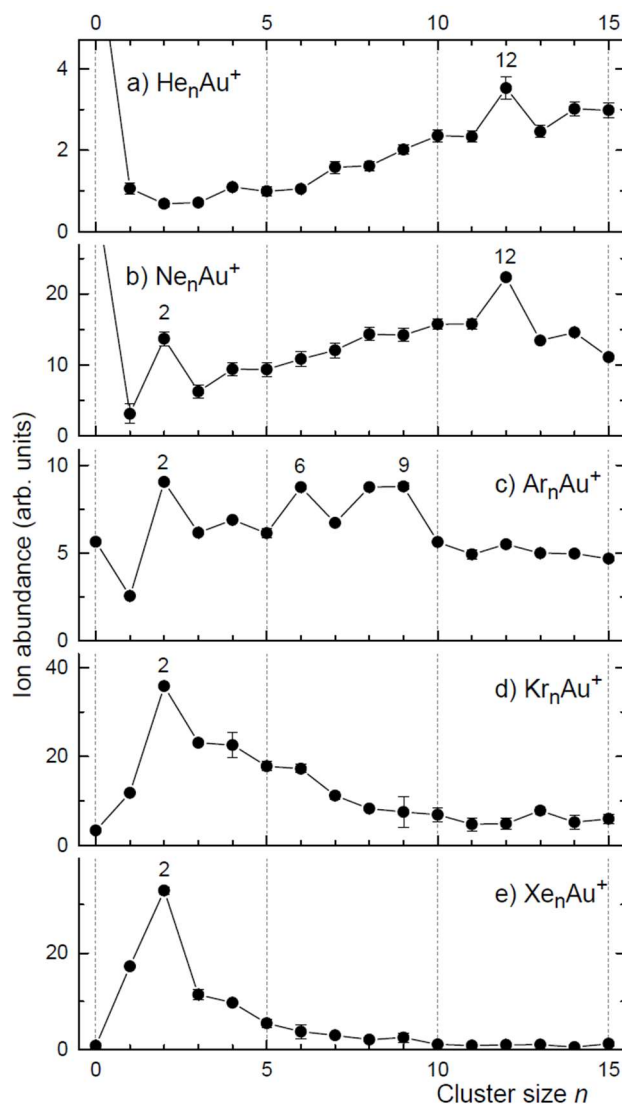


Fig. 2 Ion abundance of Ng_nAu^+ cluster ions ($\text{Ng} = \text{He}, \text{Ne}, \text{Ar}, \text{Kr}, \text{Xe}$). Significant local anomalies in the ion abundances are labeled.

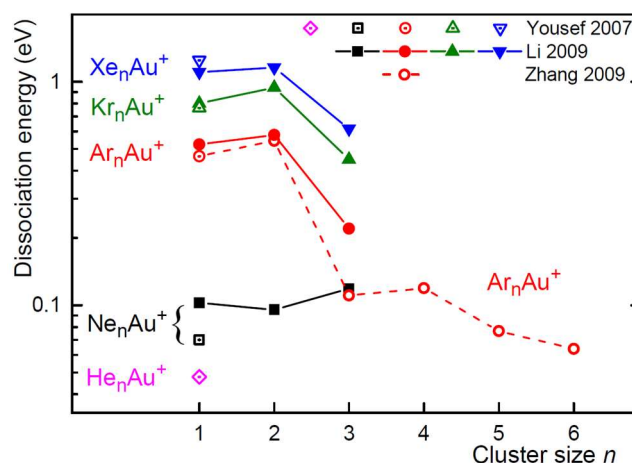


Fig. 3. Published dissociation energies calculated for Ng_nAu^+ ions. Partly filled symbols for diatomic NgAu^+ are from Yousef et al.⁹ Solid symbols connected by solid lines for Ng_nAu^+ ($n = 1, 2, 3$; $\text{Ng} = \text{Ne}, \text{Ar}, \text{Kr}, \text{Xe}$) are from Li et al.^{12,37,59,61} Open circles connected by a dashed line for Ar_nAu^+ , $n \leq 6$, are from Zhang et al.⁶²

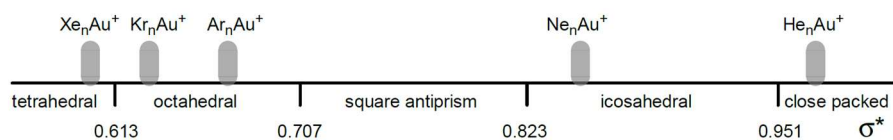


Fig. 4. Data below the abscissa indicate the structure of the first solvation shell for a metal ion (M^+) solvated in a noble gas (Ng), predicted within a hard-sphere model as a function of $\sigma^* = R_{M-Ng}/R_{Ng-Ng}$ where R_{M-Ng} is the distance between the ion and the ligand, and R_{Ng-Ng} is the distance between adjacent ligands.³⁵ σ^* values for $M^+ = Au^+$ and Ng = He, Ne, Ar, Kr, Xe are indicated above the abscissa; they are estimated from literature data (see text for details).

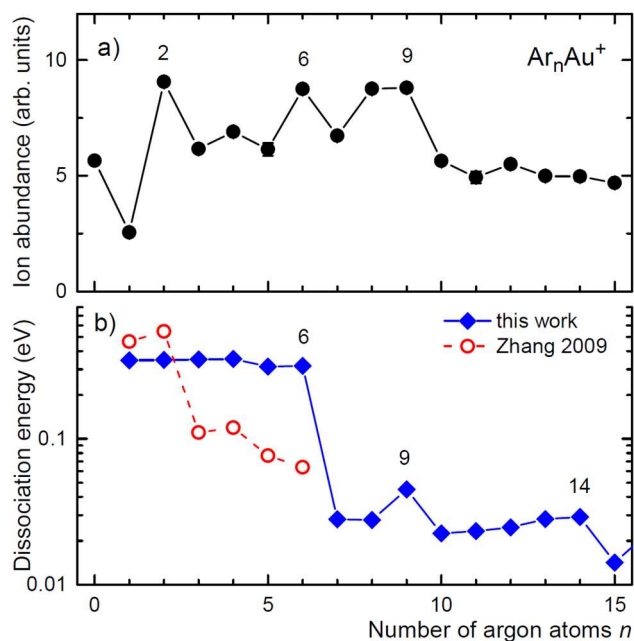


Fig. 5. Comparison of the ion abundance of Ar_nAu^+ (panel a) with calculated dissociation energies (panel b). Diamonds (this work) indicate data obtained using pairwise additive potentials. Values represented by open circles were computed at the B3LYP theoretical level by Zhang et al..⁶²

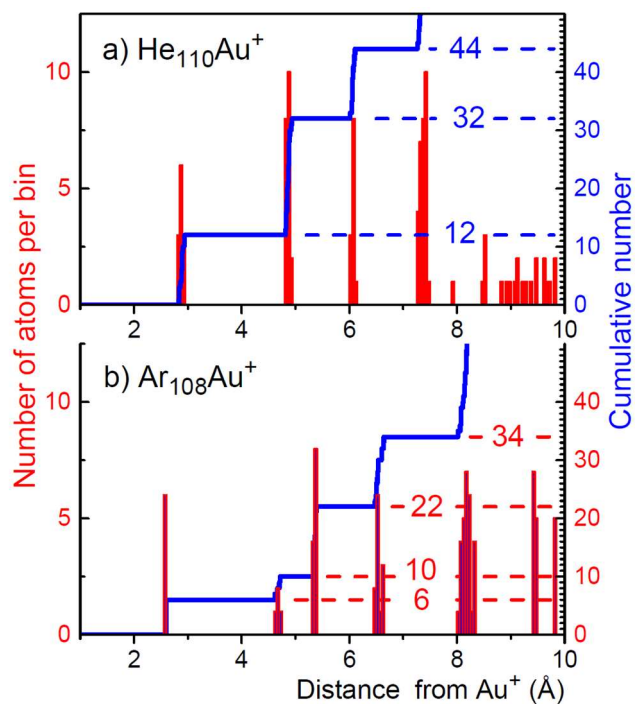


Fig. 6. The histograms (red lines) represent the computed radial helium density around Au⁺ in He₁₁₀Au⁺ and Ar₁₀₈Au⁺ (panels a and b, respectively; values are specified on the left ordinate). Blue lines represent integrated histograms, i.e. the number of He atoms within a sphere of radius r around Au⁺ (right ordinate). Values in the graph specify the cumulative number of atoms within the first, second, third,... solvation shell.